

Contents lists available at ScienceDirect

JCIS Open

journal homepage: www.journals.elsevier.com/jcis-open



Low viscosity liquid bridges: Stretching of liquid bridges immersed in a higher viscosity liquid



Ramon Lopez^a, Jovina Vaswani^a, Dylan T. Butler^b, Joseph McCarthy^a, Sachin S. Velankar^{a,c,*}

- ^a Department of Chemical and Petroleum Engineering, University of Pittsburgh, Pittsburgh, PA, 15260, USA
- ^b Department of Electrical Engineering, University of Pittsburgh, Pittsburgh, PA, 15260, USA
- ^c Department of Mechanical Engineering and Materials Science, University of Pittsburgh, Pittsburgh, PA, 15260, USA

ARTICLE INFO

Handling Editor: Kevin Roger

Keywords: Liquid bridge Viscous bridge Capillary force

ABSTRACT

We examine the dynamics of a liquid bridge between a sphere and a flat plate being separated from each other. Unlike previous research, this paper focuses on the case where the viscosity of the bridge is lower than that of the external fluid within which the particle, the plate, and the liquid bridge are immersed. For the general case of a viscosity mismatch between the bridge fluid and the external fluid, we develop a lubrication theory-based model for the viscous force during separation. The model predicts that a low viscosity bridge reduces the force as compared to both - separation without a liquid bridge, or separation with a bridge of matched viscosity. The magnitude of force reduction is expected to be more severe at small sphere-plate separations and at large bridge volumes. Experiments confirm all these predictions qualitatively, but unexpectedly the magnitude of the reduction is even larger than predicted. Experiments also find that the bridge length at rupture for specified velocity exceeds that for quasistatic rupture by an amount that increases with the squareroot of the velocity. Although we only examine bridges between a plate and a spherical particle, all results are expected to apply for bridges between a pair of particles as well.

1. Introduction

Capillary bridges spanning two solid surfaces are relevant to a wide variety of physical phenomena including the mechanics of soils or wet granular media [1,2], the use of binders in pharmaceutical tableting [3, 4], adhesion of insects to walls [5], liquid phase sintering [6], liquid transfer printing processes [7], and dip pen lithography [8]. This paper is concerned with forces developed by a liquid bridge between a spherical particle and a flat surface, when the particle is being separated from the surface at a sufficiently high speed that viscous forces play a significant role. The essential physics is equally relevant to a liquid bridge between two spherical particles undergoing separation. In contrast to previous studies on this topic, the specific situation of interest here is when the viscosity of the bridge fluid is much lower than that of the surrounding fluid.

A large body of literature has examined static liquid bridges between two solid particles or between a solid particle and a solid wall [9–12]. When the solid surfaces are fully-wetted by the bridge liquid, the bridge generally induces an attractive capillary force between the surfaces. When the solid surfaces are poorly-wetted by the liquid, the capillary

force can be repulsive [13,14]. While the above studies were done with air as the continuous phase outside the liquid bridge, similar research has also been done using two immiscible liquids, e.g. an oil bridge between particles which are immersed in water [15,16]. Other issues such as effects of contact angle hysteresis or pinning [17–19], contact angle inequality [20], size inequality [21], surface roughness [22], or gravity [23] have also been considered.

In processing operations with particulate materials however, particles are in motion with respect to each other, and viscous forces in the liquid bridge become important. For example, in a fluid bed granulator (FBG) mixer, the viscous forces in the liquid play an important role as a liquid binder is applied to a powder and mixed to form granules under a shear flow. The first step of granulation is when the binder forms liquid bridges between particles and binds them together by a combination of capillary and viscous forces [4]. If the relative velocity between the particles is large, as is common in multiple industrial processes, the viscous forces may far exceed capillary forces. Following previous studies on this topic [24,25], this situation was examined by Pitois et al. [26] who estimated the total force by summing viscous forces and capillary forces. The central assumptions of their analysis were that the viscous forces could be

^{*} Corresponding author. Dept. of Chemical Engineering, University of Pittsburgh, PA, 15260, USA. *E-mail address:* velankar@pitt.edu (S.S. Velankar).

calculated from the lubrication approximation (valid when particle separation is small), whereas the capillary forces were unaffected by particle motion, and hence identical to those under static conditions. The resulting force expression was in reasonable agreement with experiments. More recently, this same approach was applied to develop a modified capillary force model with dynamic contact angle hysteresis [27]. An excellent summary of this past research, including on the static bridges from the previous paragraph, has been tabulated by Bozkurt et al. [28].

All the research from the previous paragraph on viscous effects in liquid bridges [24-27] was conducted with air as the continuous phase fluid. There appears to be no research on the dynamics of liquid bridges for the case when the bridge has lower viscosity than the surrounding liquid. Such "viscosity-inverted" situations are not common in soil mechanics or liquid sintering, but they appear in material processing operations. For example, spherical crystallization (also called spherical agglomeration [29]) has been applied in different industrial sectors, including in the pharmaceutical industry to make tablets [30], in the food industry to remove specific particles [31], and in processing wastewater to remove heavy metals [32]. In spherical crystallization, a binder, sometimes less viscous than the continuous phase, is added to create liquid bridges between particles and produce particles agglomerates or crystals depending on the application [29,33]. Similarly, capillary forces can be used in particle suspensions to induce aggregation of particles [34]. For example, mixing a small amount of water into a suspension of hydrophilic particles in oil can induce the aggregation of particles via liquid bridges of water [35]. The resulting "pendular state" suspension can have a yield stress [36,37]. Such suspensions provide a route to material processing, e.g. to fabricate porous ceramics [38,39], especially by 3D printing [40]. Similar capillarity-driven aggregation can be induced in particle-filled polymer blends, e.g., to realize conductive plastics or adhesives [41,42]. In such cases, the fluid added to the particles may be much less viscous than the continuous phase polymer, and there is little knowledge of the behavior of such low-viscosity bridges.

This paper is a modeling and experimental study of forces associated with the stretching and rupture of low viscosity liquid bridges surrounded by a higher viscosity external fluid. In Section 2, we propose a model for the force for normal motion between a particle and a flat plate. As previously [26], the model is based on the lubrication approximation as well as geometric simplifications that are only valid at small separations. Unlike previously, the model captures both cases: when the bridge is much more viscous than the surroundings [26] or much less viscous. Section 3 describes the experimental method, and Section 4 the results for measured forces during bridge stretching. Section 5 concludes with a brief discussion and summary.

2. Theory

2.1. Viscous force

Consider the geometry (Fig. 1B) of a plate and a sphere of radius R, at a separation S_0 immersed in an outer fluid of viscosity η_o . Considering first the case without a liquid bridge, the lubrication equation using the Reynolds' approach for the pressure for normal-direction motion in an axisymmetric geometry is given by [24]

$$\frac{d}{dr}\left(rS^3(r)\frac{dP_o}{dr}\right) = 12\eta_o rv\tag{1}$$

where ν is the separation velocity and S(r) is the distance between the plate and the sphere at any radial location r. The subscript o indicates that this pressure is in the outer fluid. At close separation ($S_0 \ll R$), the geometry can be approximated by $S(r) \approx \frac{r^2}{2R} + S_0$. One can then integrate Eq. (1), set $P_o = 0$ far away (i.e. at $r \to \infty$), and $dP_o/dr = 0$ at r = 0 to yield the pressure profile $P_o(r)$

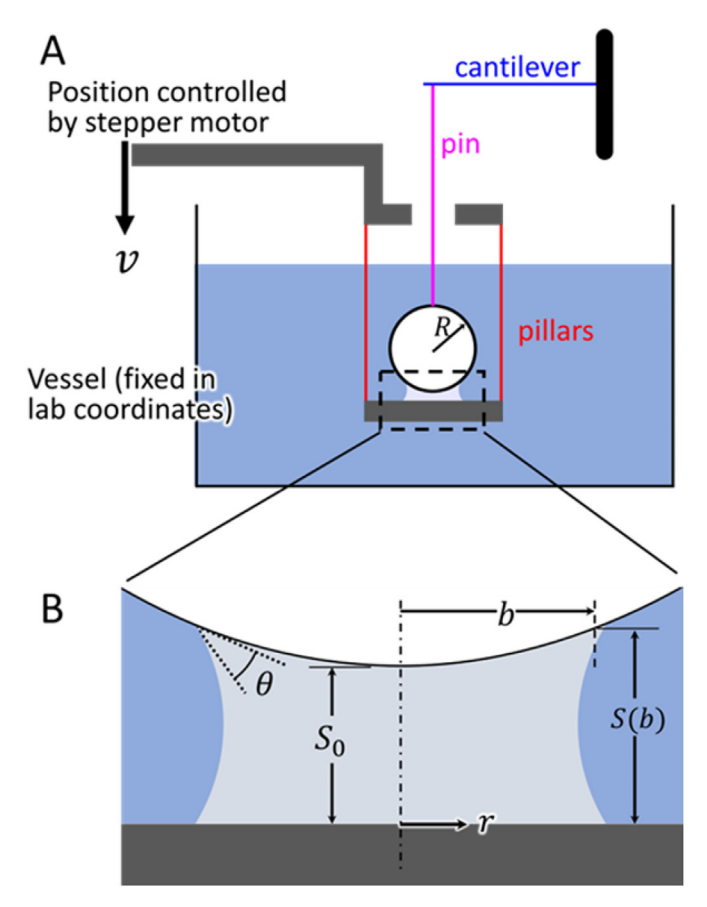


Fig. 1. Schematic of experimental apparatus for measuring the force while stretching a liquid bridge between a sphere and a plane. Note that there is no macroscopic motion of the fluid container. B. Schematic defining the various geometric quantities of the bridge. b is the radial extent of the bridge (Eq. (7)) assuming that the free surface of the bridge is cylindrical. These figures are not to scale. In experiments, R is 2 mm, the space beteen the pillars is about 20 mm, the width of the fluid container is roughly 50 mm, and S_0 ranges from 0.05 mm to 2 mm. Figure is in color in electronic version. (For interpretation of the references to color in this figure legend, the reader is referred to the Web version of this article).

$$P_o(r) = -12 \frac{\eta_o R^3 v}{(2RS_0 + r^2)^2}$$
 (2)

Integration of the above pressure profile yields the viscous force [43].

$$F_{vis} = -\frac{6\pi \eta_o R^2 v}{S_0} \tag{3}$$

Note that for positive velocity (i.e. stretching the liquid bridge), the pressure and force are both negative indicating that the force is attractive. Turning now to the geometry of Fig. 1B, consider an axisymmetric liquid bridge of viscosity $\eta_i = \eta^* \eta_o$ and volume V. Here η^* , dubbed relative viscosity, is the ratio of the viscosity of the inner to the outer fluid. For the purposes of calculating the liquid volume, we assume that the bridge has a cylindrical edge at the radial position b and height S(b), and write

$$V = \int_0^b 2\pi r S(r) dr = \pi R \left[S^2(b) - S_0^2 \right]$$
 (4)

Here the above approximation $S(r) \approx \frac{r^2}{2R} + S_0$ was used in evaluating the integral. The volume can be rendered non-dimensional as

R. Lopez et al. JCIS Open 9 (2023) 100079

$$V^* = \frac{V}{\pi R S_0^2} = \frac{S^2(b)}{S_0^2} - 1 \tag{5}$$

Accordingly, S(b) can be written in terms of non-dimensional volume as

$$S(b) = S_0 \sqrt{V^* + 1} \tag{6}$$

Further, by substituting $S(b) \approx \frac{b^2}{2R} + S_0$ into Eq. (6), one obtains

$$b = \sqrt{2RS_0\left(\sqrt{V^* + 1} - 1\right)} \tag{7}$$

Note that the non-dimensional volume V^* (Eq. (5)) depends on the separation S_0 . In contrast, previous papers on static liquid bridges often define non-dimensional volume as V/R^3 , which is independent of separation.

We will now derive the pressure profile for the case when $\eta_i \neq \eta_o$. For the outer fluid, the pressure profile is still given by Eq. (2), but only for $r \geq b$. By substituting r = b, we can obtain the pressure at the edge of the bridge

$$P_o(b) = -12 \frac{\eta_o R^3 v}{(2RS_0 + b^2)^2}$$
 (8)

For the inner fluid, Eq. (1) is still valid, but replacing η_o by η_i :

$$\frac{d}{dr}\left(rS^{3}(r)\frac{dP_{i}}{dr}\right) = 12\eta_{i}rv \quad for \ r < b$$
(9)

Here P_i is the pressure inside the bridge. Eq. (9) can be integrated, but now setting the boundary condition at the edge of the bridge as per Eq. (8) to impose continuity of pressure. This latter integral then yields

$$P_i(r) = -12 \frac{\eta_i R^3 v}{(2RS_0 + r^2)^2} + 12 \frac{(\eta_i - \eta_o) R^3 v}{(2RS_0 + b^2)^2} \quad for \ r < b$$
 (10)

Eq. (2) (for $r \ge b$) and (10) (for $r \le b$) together give the pressure profile in the entire domain. Fig. 2A–C shows the pressure profiles for three illustrative cases corresponding to $\eta^* = 0.005$, 1, and 10. The other parameters are listed in the caption of Fig. 2, and are typical of the experimental values used later in this paper. Note that ν is taken as positive, corresponding to moving the particles apart; therefore, the

pressures are negative (in fact, Fig. 2A–C plot the negative of the pressure).

Since the pressure at $r \geq b$ is given by Eq. (2) regardless of the value of η^* , the orange curve is identical in all three graphs in Fig. 2. For $\eta^* = 0.005$ (Fig. 2A), the pressure inside the bridge is nearly uniform at a value specified by the pressure at the outer edge of the bridge. In contrast, when $\eta^* = 10$, the pressure inside the bridge rises far above that at r = b. For $\eta^* = 1$, there is no discontinuity in the slope of the pressure profile, and Eq. (2) describes the pressure over the entire domain r > 0.

The total viscous force can be obtained by integrating the overall pressure profile:

$$F_{vis} = \int_0^\infty 2\pi P r dr = \int_0^b 2\pi P_i r dr + \int_b^\infty 2\pi P_o r dr$$
 (11)

The final expression is:

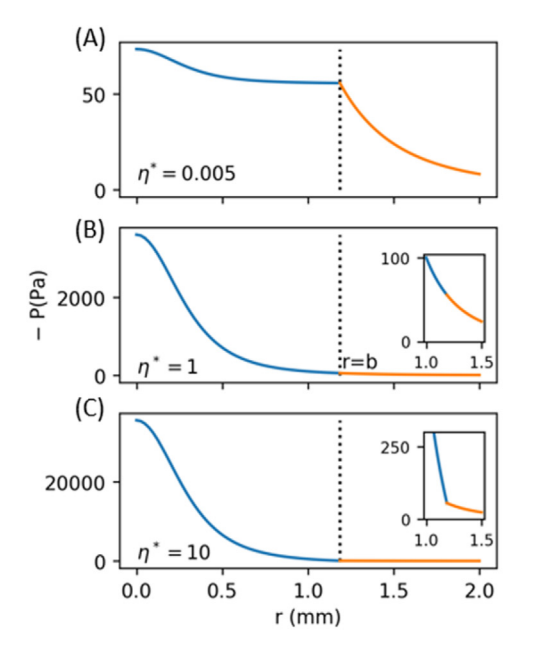
$$F_{vis} = -\frac{6\pi\eta_{o}R^{2}v}{\sqrt{\frac{v}{\pi R} + {S_{0}}^{2}}} - \frac{6\pi R^{2}v}{S_{0}} \frac{\left(\sqrt{\frac{v}{\pi R} + {S_{0}}^{2}} - S_{0}\right)\left(\eta_{i}\sqrt{\frac{v}{\pi R} + {S_{0}}^{2}} + S_{0}(\eta_{o} - \eta_{i})\right)}{\frac{v}{\pi R} + {S_{0}}^{2}}$$
(12)

Here the first and the second terms on the right hand side are the viscous contributions of the outside and bridge fluids respectively. Note that only quantities that are directly controlled experimentally appear in Eqs. (12) and (13); b and S(b) do not appear.

Rewriting F_{vis} in non-dimensional terms allows the role of various quantities to be identified clearly.

$$F_{vis} = -\frac{6\pi\eta_o R^2 v}{S_0} \left[\frac{1}{\sqrt{V^* + 1}} + \frac{\left(\sqrt{V^* + 1} - 1\right)\left(\eta^* \sqrt{V^* + 1} + 1 - \eta^*\right)}{V^* + 1} \right]$$
(13)

The quantity outside the square brackets in Eq. (13) is the viscous force in the absence of a liquid bridge (Eq. (3)). The term in the square brackets is a multiplicative factor that accounts for the geometry and viscosity of the liquid bridge, captured by the non-dimensional variables V^* and η^* respectively. This multiplicative factor is less than 1 when $\eta^* < 1$ and greater than 1 when $\eta^* > 1$. The square bracket is 1 for $V^* = 0$ (i.e. absence of a bridge) or for $\eta^* = 1$ (viscosity-matched bridge), and hence Eq. (13) reverts to Eq. (3). Eq. (13) also recovers the expression derived by Pitois [26] for $\eta_0 \ll \eta_i$.



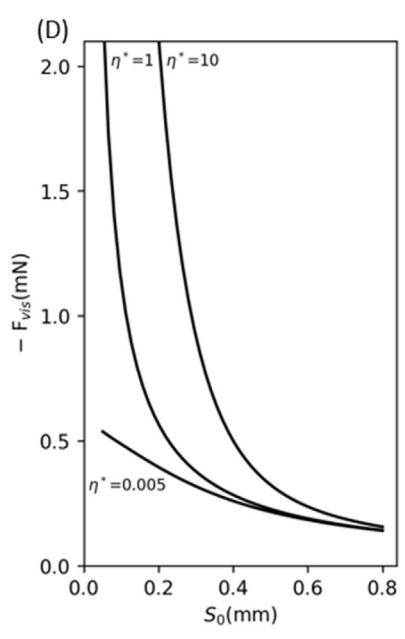


Fig. 2. A-C. Pressure profile for relative viscosity values of 0.005, 1 and 10. In all three graphs, the orange curves (i.e. r > b) are identical. Insets in B and C show a magnified view of the region near r = b. D. Evolution of viscous force as per Eq. (12) for three different values of $η^*$. For all four graphs, V = 2 μL, R = 2 mm, $η_o = 30$ Pa s, and ν = 50 μm/s. Figure is in color in electronic version. (For interpretation of the references to color in this figure legend, the reader is referred to the Web version of this article.)

Fig. 2D shows the evolution of the viscous force as per Eq. (12) as the meniscus separates. Similar to the pressure, the forces are also negative indicating attraction, and Fig. 2D plots the negative of the force. The central conclusion is that as the viscosity of the liquid bridge reduces, the viscous force needed for separation reduces to a value below that needed in the absence of the bridge. It is this regime that has not been studied previously and is the main focus of this paper. It is crucial to recognize that even if the bridge fluid were inviscid, the region covered by the bridge would still contribute to the viscous force. In this inviscid-bridge limit, the pressure inside the bridge is simply P(b) (obtained by setting $\eta_i=0$ in Eq. (10)) and hence the bridge contribution to the viscous force is $\pi b^2 P(b)$. Thus the force contribution of an inviscid bridge is proportional to the outside viscosity η_o .

We reiterate that the above analysis adopts all the three assumptions previously made by Pitois et al.: the lubrication approximation (Eq. (1)), the quadratic approximation for the geometry $S(r) \approx r^2/2R + S_0$, and the assumption that the edge of the bridge can be treated as a cylinder for calculating the volume (Eq. (4)). These assumptions require that $S_0 \ll b \ll R$, and hence the analysis is not valid when the particle-plate separation becomes large. The experiments in Section 3 go from S_0/R values of 0.025 to 0.6, but it is only in the early portion of this range (roughly $S_0/R < 0.2$) that a comparison with theory is justified.

2.2. Capillary force

The static capillary force of a small liquid bridge with fixed volume between a sphere and a plane (Fig. 1) is given by [44].

$$F_{cap} = -4\pi R\gamma \cos\theta \left(1 - \frac{1}{\sqrt{V^* + 1}}\right) \tag{14}$$

where γ is the interfacial tension, and θ is the contact angle. The above equation is only valid at relatively small contact angles (typically $\theta < 40^{\circ}$). For relatively large contact angles, the capillary force deviates from Eq. (14) and may even become repulsive [45], whereas Eq. (14) only predicts a capillary attraction between the sphere and plane. Further, the above equation is only valid while the liquid bridge is intact, i.e., when the S_0 is smaller than the static rupture distance of the liquid bridge $S_{0,stat}^{rup}$. An expression for $S_{0,stat}^{rup}$ is given in Eq. (19) later in this paper and compared with experiments.

2.3. Total force

Following Pitois [26], we assume that the total force can be obtained from the sum of the static capillary force (Eq. (14)) and the viscous force (Eq. (12)):

$$F_{tot} = F_{cap} + F_{vis} \tag{15}$$

3. Experiments

3.1. Apparatus

We seek to quantify viscous effects when the viscosity of the liquid bridge is lower than of the continuous phase. Thus, not only is the bridge submerged, but the submerging liquid has a relatively high viscosity. This requires the force-sensing mechanism (a cantilever in our case) to be mounted outside this high viscosity liquid; otherwise, viscous drag on the mechanism would affect the measurements.

Fig. 1 shows a schematic of how this was accomplished. The particle (4 mm diameter) is attached by a long pin of diameter 0.8 mm to a cantilever. The deflection of the cantilever can be measured to submicron accuracy using an optical displacement sensor (Philtec) which measures light reflected from the back of the cantilever (not shown in Fig. 1). A horizontal plate sits on a movable platform below the particle. The platform is suspended as illustrated in Fig. 1 using two "pillars" of

0.8 mm diameter each. The vertical position of the platform is controlled with a stepper motor (Moons Industries). During a typical experiment, the particle and the plate are connected by a liquid bridge with some initial separation (see Section 3.3). The stepper motor then lowers the platform at a fixed velocity ν , and the corresponding cantilever deflection is recorded. It is crucial to recognize that the particle-plate separation is changed without translating the fluid bath, thus there is negligible change in height at the upper surface of the liquid. This is essential to the current experiment; any gross motion of the air-liquid interface induces capillary and gravity forces on the surface of the pin holding the particle, which overwhelm the forces of interest. Further, it is essential that the upper surface of the particle be submerged at least several mm below the free surface of the fluid at the beginning of the experiment. If the particle breached the upper surface, or approached it closely, it significantly affected the force measurements. The apparatus is mounted in an active air vibration isolation table (Kinetic Systems).

3.2. Materials

Polyisobutylene (PIB 24, Soltex) was used as the outer continuous phase fluid in all experiments. Most experiments used polyethylene glycol (PEG, molecular weight 600 g/mol) as the low-viscosity bridge fluid. A limited number of experiments were conducted using polydimethylsiloxane (PDMS, Rhodia), whose viscosity is close to that of the PIB. The properties of each fluid used are available in Table 1. The continuous phase fluid viscosity is much higher than of water or smallmolecule organic fluids. This gives the benefit of slowing down the dynamics, which permits imaging without needing a high-speed camera. The high viscosity and low velocities also make inertial effects negligible (Reynolds numbers in these experiments are lower than 0.01).

The particles were glass spheres of diameter 4 mm. When using PEG as the bridge fluid, the particles were preferentially wetted by PEG. When using PDMS as the bridge fluid, the particles were coated with a thin layer of Sylgard 184 silicone rubber to ensure near-complete wetting by the PDMS fluid. In all cases, the contact angle was observed to be small, and $\theta=0^\circ$ was used in Eq. (14).

3.3. Experimental procedure

A drop of the bridge fluid of the desired volume was first placed on a glass slide in air with a micropipette (for PEG bridges), or with a plastic toothpick (for PDMS bridges). In the latter case, the bridge volume was determined using the drop's weight. The slide was placed on the horizontal platform. It was then immersed into the reservoir of PIB, immediately under the glass particle. The particle was brought into contact with the plate and allowed to rest for 4 min to let the bridge equilibrate. The platform was then moved downwards at a separation velocity in the range of $v=1~\mu\text{m/s}$ to 320 $\mu\text{m/s}$. The experiments were video-recorded with a Dino-Lite digital microscope. The corresponding cantilever deflection was converted into force using the cantilever spring constant.

The cantilevers were 3D-printed plates whose thickness was selected based on a tradeoff between the noisiness in the data and the maximum cantilever deflection that can be tolerated. At low speeds or under quasistatic conditions, the forces encountered were low and hence softer cantilevers were needed to achieve an adequate signal-to-noise ratio. At higher speeds, the deflection of these softer cantilevers becomes a sig-

Table 1
Liquid properties.

Liquids	Density (kg/ m ³)	Viscosity (Pa s)	Interfacial tension (mN/m) with PIB
PIB 24 PEG 600 PDMS Oil	920 1120 960	30.0 0.156 35.3	- 10.5 2.5 [46]

nificant portion of the applied displacement, which is unacceptable. Thus, higher velocities needed stiffer cantilevers. The cantilever spring constant was calibrated using deadweights hung from the cantilever at the same position as the pin holding the particle. The deflection of the cantilever was subtracted from the applied displacement to obtain the true separation S_0 .

Two validation tests of the force measurements are shown in the supplementary information: the force as a function of velocity in the absence of liquid bridges, and the force of a PEG meniscus with air as the surrounding fluid.

4. Results

4.1. Meniscus evolution during particle separation

Before discussing forces, we qualitatively show how the bridge evolves with time and discuss the effect of velocity on the meniscus evolution. A liquid bridge of $V = 5 \mu L$ of PEG 600 was added between the sphere and the glass slide, and the initial separation was set at $S_0 = 50$ μm. A first experiment was conducted at a separation velocity v = 1 μm/ s, and the images in Fig. 3A-D were recorded. The initial separation was then reset to $50 \, \mu m$, and the liquid bridge allowed to equilibrate for $4 \, min$ before the experiment was repeated at $v = 100 \, \mu \text{m/s}$, and the images in Fig. 3 E-H were recorded. The recession of the bridge is clearly different in both cases. At low velocity, the bridge has more time for equilibration (indeed we will show later that this experiment may be regarded as quasistatic). Accordingly, the bridge fluid is sucked out of the liquid bridge, both due to capillarity as well as gravity, leading to a thin bridge which ruptures when S_0 is roughly 1600 µm. In contrast, high separation velocity results in a fatter liquid bridge which does not rupture even at $S_0 =$ $2000 \ \mu m$. This increase in rupture distance with velocity will be covered in detail in Section 4.5.

In all experiments, a portion of the bridge fluid remains as a layer on the bottom of the particle, whereas a larger portion remains coated on the plate, presumably due to gravitational effects. One may compare the magnitude of gravity (roughly on the order of the hydrostatic stress Δ $\rho gS(b)$ where $\Delta\rho$ is the density difference between the fluids) and the viscous stresses (on the order of $P_o(b)\sim 3\eta_0Rv/S(b)^2$ from Eq. (8)). This comparison suggests that at the beginning of the experiment, viscous forces dominate over gravity at all except the lowest experimental velocities tested. With decreasing velocity or increasing separation, gravitational effects are expected to become more important. Since the bridge fluid has higher density than the surrounding PIB, gravity induces the

bridge to sag downward. Indeed, it was found that the portion of bridge fluid left on the plate increased with decreasing separation velocity. This trend has been reported previously for liquid bridges between two flat plates [47], and indicates that gravity has more influence at low velocity. The influence of gravity in the limit of low velocity can be captured by the Bond number, which is the ratio of gravitational force to the surface tension force in the liquid bridge:

$$Bo = \frac{V^{\frac{2}{3}}\Delta\rho g}{\gamma} \tag{16}$$

where $\Delta \rho$ is the density difference, and g is the acceleration constant. For the V values in this paper $(1-5~\mu L)$ the Bond number is in the range of 0.22–0.65. Incidentally it is common to instead define a Bond number based on the dimension b. If we define Bo as $\frac{b^2\Delta\rho g}{\gamma}$, then using the b values calculated from Eq. (7) at a separation distance of 50 μm , the Bo values are in range of 0.3–0.72. With either definition, Bo is on the order of 1 suggesting a moderate effect of the gravitational forces, at least under static conditions.

4.2. Effect of bridge viscosity on the force during separation

The key issue of interest here is how low viscosity bridges affect the total liquid bridge force. Fig. 4 illustrates the main effects qualitatively. We compare the measured force in three cases: no bridge, viscosity-matched bridge (PDMS), and low viscosity bridge (PEG) where the latter two have roughly comparable volumes. In all cases, the separation velocity was $\nu=100~\mu\text{m/s}$, and the initial separation was $S_0=50~\mu\text{m}$. As will be shown later, at this velocity, capillary forces are much smaller than viscous forces, thus allowing the effects of bridge viscosity to be identified clearly.

In the absence of the liquid bridge, the separation force follows Eq. (3), as may be expected from the more comprehensive set of data for the no-bridge case in Fig. S1. For the nearly viscosity-matched liquid bridge, the viscous contribution to the force is nearly identical to that from Eq. (3). The total force is in reasonable agreement with Eq. (15). Remarkably, the theory is in reasonable agreement with the experiments throughout the range of separations even though (as mentioned in Section 2.1), the lubrication approximation requires $S_0 \ll R$.

In contrast, the low viscosity bridge shows much lower forces at small separations, which is in qualitative agreement with the theoretical model. To our knowledge, this is the first documentation in the literature of a low viscosity liquid bridge lowering the total force during separation.

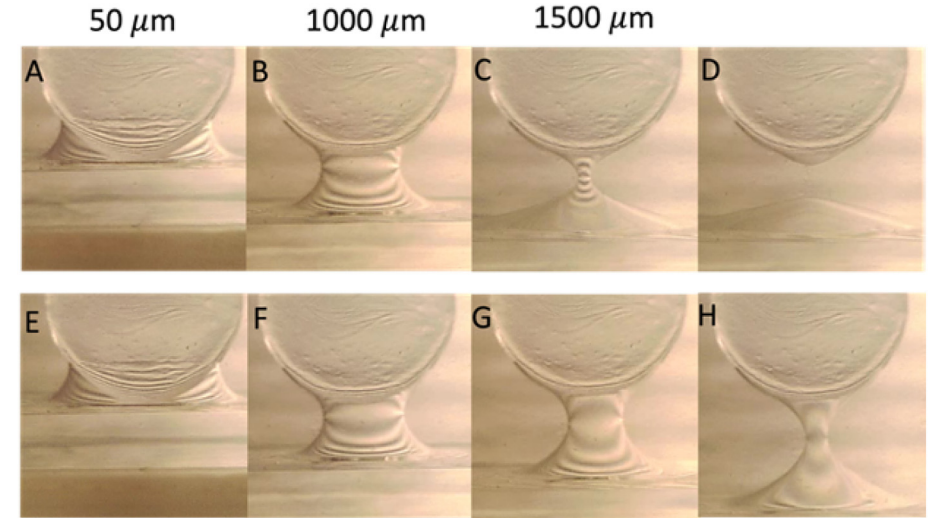


Fig. 3. Liquid bridge of PEG 600 with a volume V=5 μL undergoing separation at velocity v=1 μm/s (upper row) and v=100 μm/s (lower row). The S_0 values for the first three images in each row are listed at the top. Image D is at $S_0=1557$ μm, immediately after rupture. Image H corresponds to $S_0=2000$ μm and the bridge has not yet ruptured. A horizontal stripe pattern is placed in the background to accentuate the edge of the bridge. Figure is in color in electronic version. (For interpretation of the references to color in this figure legend, the reader is referred to the Web version of this article.)

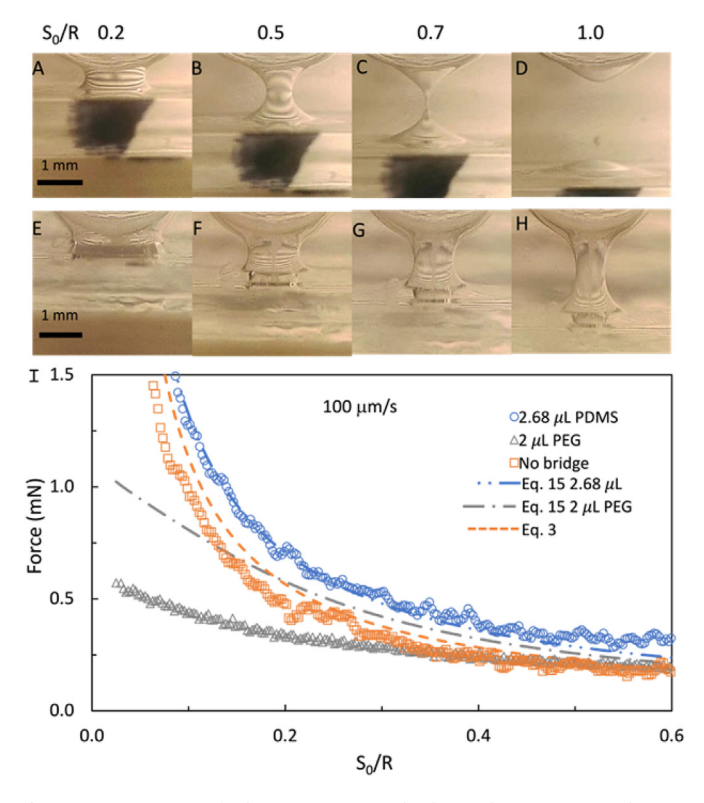


Fig. 4. (A–D) Images of a low-viscosity PEG bridge with $V=2~\mu L$, and (E–H) images of a viscosity-matched PDMS bridge of $V=2.68~\mu L$ at different S_0/R values (labeled at the top of each column). In both cases, the continuous fluid was PIB. The dark black region in A-D is an ink-mark made on the front edge of the bottom plate and does not interfere with this experiment. It was placed during early experiments to track motion of the bottom plate. I) Total force during separation for both bridges and for a no-bridge case, all at a separation velocity of $v=100~\mu m/s$. Lines are predictions of Eq. (15), with line color matching the corresponding symbol color. Although Eq. (15) is plotted across the entire range of S_0/R values, the approximations underpinning Eq. (15) are only valid for relatively small S_0/R values (see Section 3.1). Figure is in color in electronic version. (For interpretation of the references to color in this figure legend, the reader is referred to the Web version of this article.)

Quantitatively however, Eq. (15) overestimates the total force for the case of low viscosity meniscus by a factor of \sim 2. This will be discussed further in Section 5.

The rest of this article only examines the case of the low viscosity liquid bridge, first examining the effect of separation velocity, and then of the meniscus volume.

4.3. Effect of velocity

Fig. 5A shows the effect of separation velocity on the force evolution for the low viscosity PEG bridge at a bridge volume of $V=2~\mu L$. The force increases with increasing velocity indicating increasing viscous contributions. In contrast, the capillary contributions are expected to depend primarily on separation; in fact, the model assumes that the capillary force is equal to the static capillary force, and therefore is velocity-independent. Accordingly, Eq. (15) has the form $F_{tot}=F_{cap}+A\nu$ where F_{cap} and A both depend on S_0 but not on ν . Therefore, two regimes may be distinguished: a viscosity-dominated regime with $F_{tot} \propto \nu$ and a capillary-dominated regime with F_{tot} being independent of ν . The former regime may be identified by testing whether the measured $F_{tot}/\nu \approx S_0$ is independent of ν . The corresponding plot, Fig. 5B shows that speeds above $\nu=60~\mu\text{m/s}$ are viscosity-dominated, whereas below that velocity, surface tension makes a significant contribution to the total force. In the viscosity-dominated regime, the total force F_{tot} in Eq. (15) may be

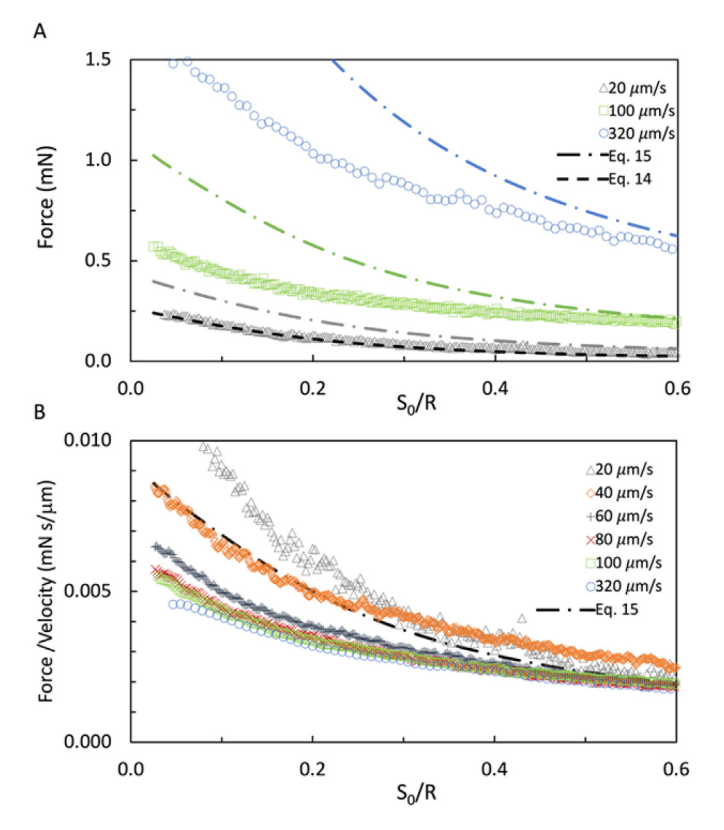


Fig. 5. A) Force curves during separation for a liquid bridge of volume $V=2~\mu L$ at different separation velocities and the predictions of Eq. (15) (dot-dashed lines, where the line color corresponds to each symbol color). B) Ratio of the force divided by velocity compared to the total force Eq. (15). Although Eq. (15) is plotted across the entire range of S_0/R values, the approximations underpinning Eq. (15) are only valid for relatively small S_0/R values (see Section 3.1). Figure is in color in electronic version. (For interpretation of the references to color in this figure legend, the reader is referred to the Web version of this article.)

approximated as F_{vis} (Eq. (13)) since the capillary force is negligible; however, Fig. 5B shows that the data lie significantly below the model. This is discussed further in Section 5.

4.4. Effect of bridge volume

Finally, we turn to examining the effect of bridge volume on the separation forces. Eq. (15) predicts that with increasing bridge volume, the viscous contribution to the separation force decreases. This is because the bridge spans a wider region (i.e. a larger V implies a larger b, Eq. (7)), and hence more of the near-contact region is occupied by the low viscosity fluid. On the other hand, a larger bridge volume raises the rupture distance S_0^{rup} , and allows the capillary force to persist to larger values of S_0 . Thus, experiments must be conducted at both high and low velocities to evaluate the differing effects in the viscosity-dominated vs capillary-dominated regimes.

Fig. 6A shows that at high velocity, the separation force is much lower than the case without a liquid bridge as also shown previously in Fig. 4. Further, the magnitude of decrease in force increases with increasing bridge volume. Beyond a nondimensional separation of about S_0/R of 0.6, all three volumes have comparable forces suggesting that the bridge makes little contribution to the total force at larger separations.

In the opposite extreme, at $v=5~\mu\text{m/s}$, the situation is reversed. The viscous forces are relatively small, and for the $V=5~\mu\text{L}$ liquid bridge, the separation force exceeds that of the no-bridge case, and further, the force decreases only gradually as separation increases. This is a consequence of the relatively large bridge volume which allows the bridge to survive

R. Lopez et al. JCIS Open 9 (2023) 100079

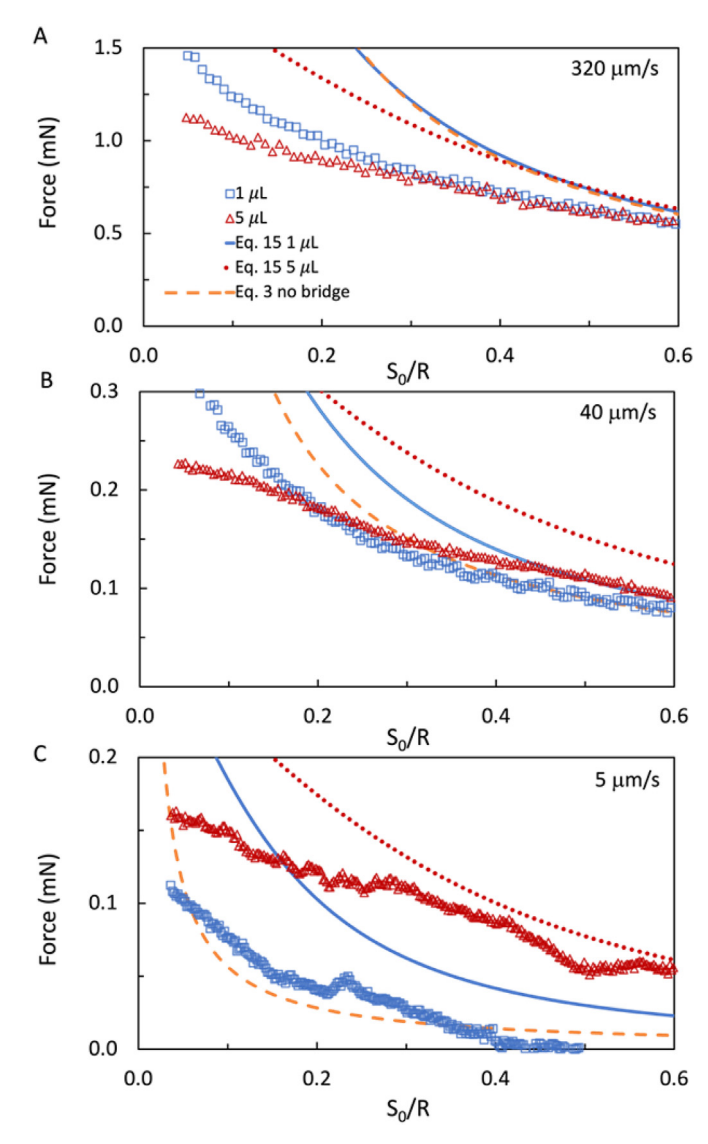


Fig. 6. The total force exerted in a particle with a PEG bridge volume of V=1 μL, 5 μL and no-bridge using a separation velocity of A) $\nu=320$ μm/s, B) 40 μm/s and C) 5 μm/s). Note that the y-scale changes several fold going from A to C. Although Eq. (15) is plotted across the entire range of S_0/R values, the approximations underpinning Eq. (15) are only valid for relatively small S_0/R values (see Section 3.1). Figure is in color in electronic version. (For interpretation of the references to color in this figure legend, the reader is referred to the Web version of this article.)

without rupturing up to a large separation. Similar results were observed previously in the capillary force dominated regime for the case of a viscous meniscus with air as the surrounding fluid [26,48]. At lower bridge volume $V=1~\mu L$, the force approaches zero because the bridge ruptures beyond $S_0/R=0.5$, and the viscous forces are small at $\nu=5~\mu m/s$.

The case of $\nu=40~\mu\text{m/s}$ appears intermediate between these two extremes. The liquid bridge reduces the force at small separations when viscous force dominates, but not at large separations. Indeed at large separation, the bridge may increase the force slightly because of capillary contributions.

4.5. Liquid bridge rupture distance

Finally, our experiments also show the velocity-dependence of the distance S_0^{rup} at which the liquid bridge ruptures. These are shown in Fig. 7A for bridges of volume of V=1 and 5 μ L. The maximum velocity

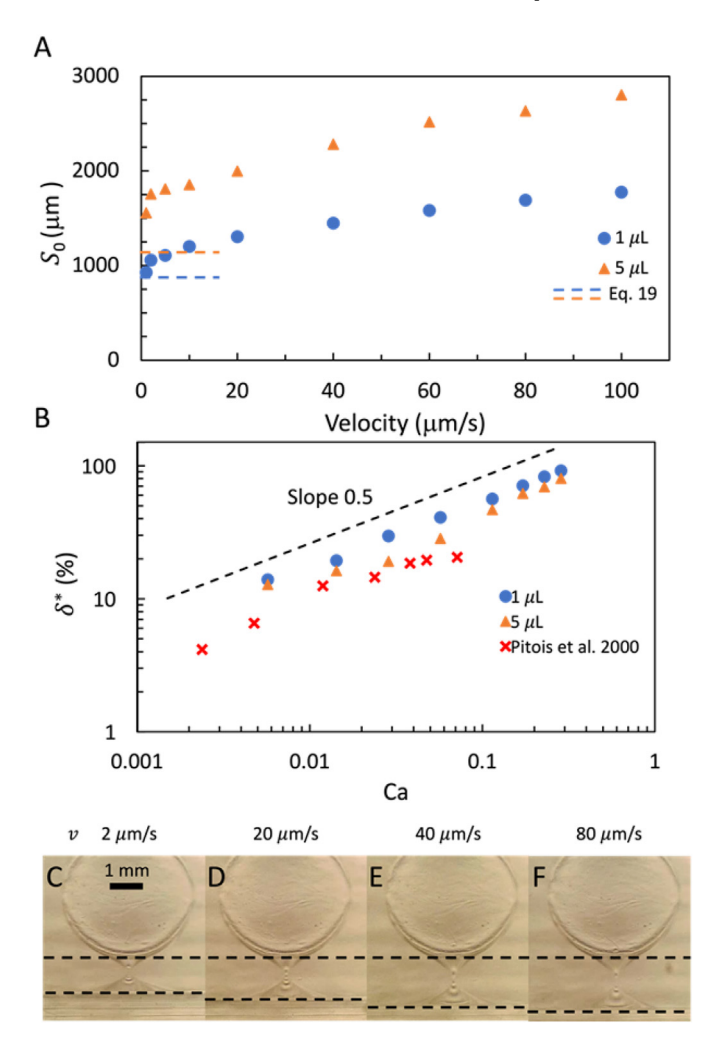


Fig. 7. A) Rupture distance (S_0^{rup}) as a function of separation velocity and B) normalized rupture distance (S_0^{**}) vs capillary number for a PEG liquid bridge. C-E. Images of liquid bridge immediately prior to rupture at different velocities C) $\nu=2~\mu\text{m/s}$, D) 20 $\mu\text{m/s}$ E) 40 $\mu\text{m/s}$ and F) 80 $\mu\text{m/s}$. Dashed lines, indicating the edge of the particle and the location of the plate, illustrate the increase in rupture distance with velocity. Figure is in color in electronic version. (For interpretation of the references to color in this figure legend, the reader is referred to the Web version of this article.)

shown in Fig. 7A is $\nu=100~\mu m/s$ since beyond this velocity, the liquid bridge draws into a very thin filament prior to breaking, making it difficult to determine the precise instant at which the liquid bridge breaks. At both bridge volumes, the rupture distance increases significantly as velocity increases. Similar results have been seen by Pitois et al. [26] for viscous bridges between particles, and by Zhang and Basaran for inertial bridges between parallel plates [47].

Pitois et al. [26] observed that for a liquid bridge of high relative viscosity, the results could be well-captured by

$$S_0^{rup} - S_{0 stat}^{rup} \propto v^{\frac{1}{2}} \tag{17}$$

where S_0^{rup} is the rupture distance at static conditions, i.e. in the limit of $v \to 0$. Eq. (17) can be written in non-dimensional terms as

$$\delta^* = \frac{S_0^{rup} - S_{0 \text{ stat}}^{rup}}{S_{0 \text{ stat}}^{rup}} \propto Ca^{\frac{1}{2}}$$
 (18)

where $Ca = \nu \eta_0 / \gamma$ is the capillary number, and δ^* is the fractional increase in rupture distance over its static value.

For a plate-sphere configuration, the rupture distance $S_{0 \text{ stat}}^{rup}$ is given by [49]

$$S_{0,stat}^{rup} = \left(1 + \frac{\theta}{4}\right) \left[\left(\frac{V}{R^3}\right)^{\frac{1}{3}} - \frac{2}{5} \left(\frac{V}{R^3}\right)^{\frac{2}{3}} \right]$$
 (19)

The values of $S_{0,stat}^{rup}$ calculated from Eq. (19) are in reasonable agreement with those measured at $\nu=1$ µm/s, suggesting that this velocity is near quasi-static conditions. We therefore adopt the values of S_0^{rup} at $\nu=1$ µm/s as static rupture distance $S_{0,stat}^{rup}$. The δ^* thus-calculated (expressed as a percentage) are plotted against Ca in Fig. 7B, and are in reasonable agreement with the square root dependence Eq. (17).

Fig. 7B shows that the δ^* for high viscosity bridges measured previously [26] are much lower than our measurements. However the comparison is not exact for two reasons: first we use $Ca = \nu \eta_o / \gamma$ whereas for a high viscosity bridge, it is necessary to define $Ca = \nu \eta_i / \gamma$; and second the value of V^* is not identical in our experiments vs [26]. Regardless, our results show relatively large magnitudes of δ^* , approaching 100%. In contrast, the largest value of δ^* noted by Pitois [26] was about 10%.

5. Discussion

To summarize briefly, the model and experiments both show that the forces needed to elongate a liquid bridge between a plate and sphere decrease significantly when the liquid bridge has a much lower viscosity than the surrounding fluid. This section addresses two issues.

The first is the distinction between viscous-dominated vs capillary-dominated regimes of separation. In Fig. 5B, this distinction was made empirically based on whether the total force is proportional to velocity or not. A theoretical approach however is to take the ratio of the viscous to capillary forces, which, based on Eqs. (12) and (14), result in an equation of the form

$$\frac{F_{vis}}{F_{cap}} = \frac{v \eta_o}{\gamma} \frac{R}{S_0} \mathcal{F}(V^*, \eta^*) = Ca \frac{R}{S_0} \mathcal{F}(V^*, \eta^*)$$
(20)

The function \mathcal{F} can be deduced from Eqs. (12) and (14). In some situations, e.g. coating operations, breakup of drops and bubbles, the viscous-dominated vs capillary-dominated regimes may be identified solely based on whether Ca is much larger or much less than 1. In the present situation however, it is clear that the ratio of viscous to capillary forces increases as S_0 reduces. Accordingly, if the particles are initially in contact with $S_0 = 0$ (which would generally be the case for freelysuspended smooth particles bonded by a liquid bridge), Eq. (20) predicts the separation process *always* starts in a viscosity-dominated regime no matter how small the velocity. During the separation process, F_{vis}/F_{cap} may become less than 1, i.e. the separation process may transition to a capillary-dominated regime as was indeed noted previously [26]. This point – that the initial separation is always viscosity-dominated – applies regardless of whether η_o is more or less than η_i , and does not appear to be emphasized in the previous literature. We caution however that this conclusion is strictly valid only for perfectly-smooth particles, whereas particles in contact have an average separation S_0 that is on the order of particle roughness. Nevertheless, as long as the roughness is small (i.e. R/ S_0 is large), Eq. (20) predicts that F_{vis}/F_{cap} would be a large, i.e. early stages of separation are more likely to be viscosity-dominated.

The second is the discrepancy between predictions and experiment. One may intuitively expect, and indeed Eqs. (12) and (13) predict, that a low viscosity bridge would reduce the force required for separation. While this is observed experimentally, the observed effect is even larger than predicted: for low viscosity bridges separated at relatively high speeds (Fig. 5), the experimentally-measured forces are typically 2x smaller than the predictions. At the high velocities in Fig. 5, $F_{cap} \ll F_{vis}$ suggesting that it is the F_{vis} that is underpredicted. In fact, the $\sim 2x$ underprediction remains even at small separations when the lubrication

approximation, Eq. (1), and the geometric approximations leading to Eq. (7) are most likely to be valid. In contrast, Eq. (12) is in good agreement with experiments for a viscosity-matched bridge (Fig. 4), and/or for a high viscosity bridge [26]. While we are not able to explain this discrepancy, we speculate that it is attributable to a failure of Eq. (15).

Eq. (15) is based on two assumptions. The first is that the capillary force remains equal to its static value (Eq. (14)) regardless of separation velocity. The second is that viscous forces are decoupled from the capillary forces (i.e. viscous forces are unaffected by capillary phenomena at the edge of the bridge). Yet, these assumptions may be violated as illustrated in Fig. 8.

Fig. 8A sketches the initial static configuration of the bridge. For quasistatic separation, the contact line of the liquid bridge recedes as the separation distance increases (compare Fig. 8A and B). Furthermore, quasistatic separation means that the interface remains in mechanical equilibrium such that the interfacial curvature in Fig. 8B matches that under static conditions at the same value of S_0 . Since the radial extent of the bridge and its curvature are both equal to the static case, the F_{cap} remains equal to the static value. Viscous forces are of course negligible under quasistatic conditions.

As velocity increases, the capillary and viscous forces may affect each other in a complex manner. Fig. 8C illustrates a possible scenario where the contact line does not recede, but instead a thin residual coating of the bridge is left behind on the plate and on the sphere such that the contact is pinned nearly to its original location (compare Fig. 8A and C). In the scenario of Fig. 8C, the interfacial curvature and the extent of the bridge both deviate from the static value, and hence F_{cap} would become velocity-dependent. Further, since the bridge liquid has a low viscosity ($\eta^* = 0.005$ here), the thin residual coating may provide excellent lubrication. In the context of Fig. 2, the viscous pressure would become independent of r over a larger region, which would reduce the force needed for the separation as compared to the model of Section 2.1. We emphasize that a thin coating of the bridge fluid may be left behind regardless of η^* . However, when $\eta^* \gg 1$, e.g. when the outside fluid is air, this thin coating would not affect the fluid mechanics in the bridge region

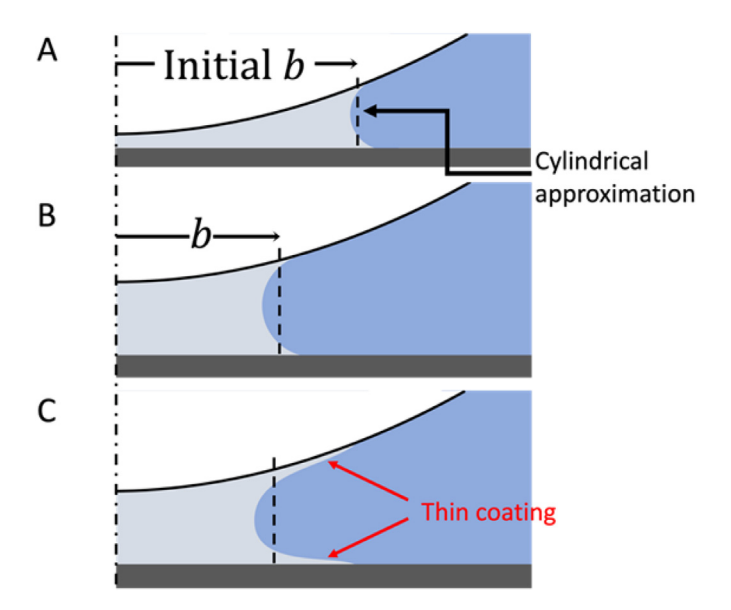


Fig. 8. Liquid bridge at A) initial configuration, and B) after some separation assuming that the contact line recedes along both solid surfaces. C) A thin residual coating of the bridge liquid remains on the sphere and the plate. The vertical dashed lines correpond to cylindrical surfaces enclosing the same volume as the bridge (Eq. (7)). Note that in C, the separation distance is identical to that in B, but the contact line on the sphere and the plate is still at its initial value in A. Figure is in color in electronic version. (For interpretation of the references to color in this figure legend, the reader is referred to the Web version of this article.)

or separation force. It is only when the bridge has low viscosity that this thin coating affects the separation force.

To summarize the above speculation, the assumptions underlying Eq. (15) would fail if the contact line does not recede as expected. This would make F_{cap} dependent on velocity, and make F_{vis} dependent on capillary phenomena. The first step to test the physical picture of Fig. 8 would be direct visualization of the three-phase contact lines. That is not viable with the imaging method used in this paper; instead, imaging along the z-direction, perhaps with tracer particles added to the bridge fluid, may be necessary.

However, we note that even though the idea of a thin residual coating is appealing, it is unlikely to be the sole reason for the discrepancy. This is because the model overpredicts the force right from the beginning of the separation, whereas the notion of a residual coating is meaningful only after some separation. It is possible that the velocity field in the outer fluid is significantly perturbed by the interface, whereas the lubrication model of course presumes a parabolic velocity profile at all locations. More precise modeling, possibly informed by computational results, may be needed to explain why the model overpredicts the separation force.

6. Summary and conclusion

This paper examines the dynamics of a liquid bridge between a sphere and a flat plate being separated from each other. The total force needed for separation has contributions from both, viscous as well as capillary forces. Unlike previous research in this area [24–26,28] this paper focuses on situations where the viscosity of the bridge is far lower than of the external fluid within which the particle and the plate are immersed. We hypothesize that such low viscosity bridges reduce the force when the separation velocity is sufficiently large that viscous forces make a significant contribution.

We develop a theoretical model for the total force during separation. Similar to previous research [26] the total force is postulated to be a sum of the capillary force (assumed to be equal to the static capillary force) and the viscous force. The latter is calculated using the lubrication approximation, and hence the model is justified only when the particle-plate separation is much smaller than the particle radius. Unlike previous research where the external fluid was assumed to be inviscid [24-26], the model in this paper is valid at any ratio of viscosity of the bridge fluid to the external fluid. The total force thus calculated includes viscous contributions from both, the pressure outside the liquid bridge (proportional to the viscosity of the outside fluid), and from the pressure inside the liquid bridge. In the case of interest here, when the bridge viscosity is low, the model predicts that the pressure in the bridge is nearly constant and has a value that is governed entirely by the external fluid. Crucially, the bridge region is predicted to contribute to the viscous force even if the bridge fluid is inviscid. As hypothesized, the model predicts that a low viscosity bridge reduces the separation force as compared to both, separation with a bridge of matched viscosity, or separation without a liquid bridge.

The model is compared with experiments in which a sphere is separated from a flat plate at a specified velocity. Unlike previous literature on force measurements of liquid bridges [see the numerous citations reviewed in Refs. [10,28]], in the present situation, the external fluid has high viscosity. Thus, any macroscopic motion of the external fluid leads to additional forces beyond those in the liquid bridge which can obfuscate measurements. To eliminate these, a new apparatus was designed wherein the sphere-plate separation could be changed without macroscopic motion of the external fluid container. Experiments confirm that a low-viscosity bridge reduces the total force during separation, and that the magnitude of force reduction increases as the bridge volume increases or as sphere-plate separation reduces. To our knowledge, this is the first report of a liquid bridge reducing the force needed to separate two surfaces. This experimental observation is most obvious at small separations at which the geometric assumptions underpinning the theory are well-justified. The magnitude of force reduction is almost two-fold

larger than predicted by the model. Although we are not able to fully explain this discrepancy, we speculate that one reason for the discrepancy is that the contact line may not recede as expected as the solid surfaces separate from each other. Finally, experiments on low viscosity bridges also show that the bridge length at rupture at specified velocity exceeds that for quasistatic rupture by an amount that increases with the square root of the velocity. This same square root dependence was noted previously [26] for high viscosity bridges suggesting that it is universal, i.e. valid regardless of viscosity mismatch.

Although experiments are conducted and the theory is derived for bridges between a plate and a spherical particle, all results are expected to apply for bridges between a pair of particles as well. Thus these results are immediately relevant to particulate suspensions in which a wetting fluid is used to induce aggregation of the particles by liquid bridges, often into a space-spanning network [34,38,50]. Such suspensions typically have a yield stress, making them useful in applications such as extrusion-based 3D printing. The rheology of these suspensions, which is critical to their applications for materials processing, is governed by the micromechanics of breaking liquid bridges between particles. These results suggest that low viscosity bridges may facilitate flow of these suspensions at a specified rate while leaving unaffected their yield stress which depends on static capillary forces.

Funding

SV and JV acknowledge support from NSF Grant #2031144. DB and SV acknowledge support from NSF Grant #1824708 and #2036164. RL acknowledges support of the AFOSR under BAA No. STTR 16. C/MDA16-T001

Author contributions

RL, SV, and JJM conceptualized the research. SV and DB designed and constructed the platform. RL, JV, and SV developed the lubrication model. RL conducted and analyzed the experiments. RL, JV, JJM, and SV contributed to writing the paper.

Declaration of competing interest

The authors declare that they have no known competing financial interests or personal relationships that could have appeared to influence the work reported in this paper.

Data availability

Data will be made available on request.

Appendix A. Supplementary data

Supplementary data to this article can be found online at https://doi.org/10.1016/j.jciso.2023.100079.

References

- [1] J. Bachmann, R.R. van der Ploeg, A review on recent developments in soil water retention theory: interfacial tension and temperature effects, in: Journal of Plant Nutrition and Soil Science, 2002, p. 4, https://doi.org/10.1002/1522-2624(200208)165:4<468::AID.JPI.N468>3.0.C0:2-G. 165.
- [2] J. Chen, K. Williams, W. Chen, J. Shen, F. Ye, A review of moisture migration in bulk material, Part. Sci. Technol. 38 (2020), https://doi.org/10.1080/ 02726351.2018.1504152.
- [3] J.D. Litster, K.P. Hapgood, J.N. Michaels, A. Sims, M. Roberts, S.K. Kameneni, Scaleup of mixer granulators for effective liquid distribution, Powder Technol. 124 (2002), https://doi.org/10.1016/S0032-5910(02)00023-2.
- [4] S.M. Iveson, J.D. Litster, K. Hapgood, B.J. Ennis, Nucleation, growth and breakage phenomena in agitated wet granulation processes: a review, Powder Technol. 117 (2001) 1–2, https://doi.org/10.1016/S0032-5910(01)00313-8.
- [5] J.H. Dirks, W. Federle, Fluid-based adhesion in insects principles and challenges, Soft Matter 7 (2011) 23, https://doi.org/10.1039/c1sm06269g.

- [6] R.M. German, P. Suri, S.J. Park, Review: liquid phase sintering, J. Mater. Sci. 44 (1) (2009), https://doi.org/10.1007/s10853-008-3008-0.
- [7] S. Kumar, Liquid transfer in printing processes: liquid bridges with moving contact lines, Annu. Rev. Fluid Mech. 47 (2015), https://doi.org/10.1146/annurev-fluid-010814-014620.
- [8] B. Godin, et al., Dip-pen nanolithography, in: Encyclopedia of Nanotechnology, 2012, https://doi.org/10.1007/978-90-481-9751-4_282.
- [9] H.J. Butt, M. Kappl, Surface and Interfacial Forces (2010), https://doi.org/ 10.1002/9783527629411.
- [10] G. Lian, J. Seville, The capillary bridge between two spheres: new closed-form equations in a two century old problem, Adv. Colloid Interface Sci. 227 (2016), https://doi.org/10.1016/j.cis.2015.11.003.
- [11] P.A. Kralchevsky, N.D. Denkov, Capillary forces and structuring in layers of colloid particles, Curr. Opin. Colloid Interface Sci. 6 (4) (2001), https://doi.org/10.1016/ S1359-0294(01)00105-4.
- [12] B. Harimi, M.H. Ghazanfari, M. Masihi, Modeling of capillary pressure in horizontal rough-walled fractures in the presence of liquid bridges, J. Pet. Sci. Eng. 185 (2020), https://doi.org/10.1016/j.petrol.2019.106642.
- [13] D. Megias-Alguacil, L.J. Gauckler, Capillary forces between two solid spheres linked by a concave liquid bridge: regions of existence and forces mapping, AIChE J. 55 (5) (2009), https://doi.org/10.1002/aic.11726.
- [14] W. Peng, B. Bhushan, A numerical three-dimensional model for the contact of layered elastic/plastic solids with rough surfaces by a variational principle, J. Tribol. 123 (2001) 2, https://doi.org/10.1115/1.1308004.
- [15] G. Mason, W.C. Clark, Liquid bridges between spheres, Chem. Eng. Sci. 20 (1965) 10, https://doi.org/10.1016/0009-2509(65)80082-3.
- [16] D. Rossetti, X. Pepin, S.J.R. Simons, Rupture energy and wetting behavior of pendular liquid bridges in relation to the spherical agglomeration process, J. Colloid Interface Sci. 261 (1) (2003), https://doi.org/10.1016/S0021-9797(03) 00043-2
- [17] X. Pepin, D. Rossetti, S.M. Iveson, S.J.R. Simons, Modeling the evolution and rupture of pendular liquid bridges in the presence of large wetting hysteresis, J. Colloid Interface Sci. 232 (2) (2000), https://doi.org/10.1006/jcis.2000.7182.
- [18] H. Chen, A. Amirfazli, T. Tang, Modeling liquid bridge between surfaces with contact angle hysteresis, Langmuir 29 (10) (2013), https://doi.org/10.1021/ la304870h.
- [19] H. Chen, T. Tang, H. Zhao, K.Y. Law, A. Amirfazli, How pinning and contact angle hysteresis govern quasi-static liquid drop transfer, Soft Matter 12 (7) (2016), https://doi.org/10.1039/c5sm02451j.
- [20] C.F. Zhao, N.P. Kruyt, O. Millet, Capillary bridges between unequal-sized spherical particles: rupture distances and capillary forces, Powder Technol. 346 (2019), https://doi.org/10.1016/j.powtec.2019.02.015.
- [21] H.N.G. Nguyen, O. Millet, G. Gagneux, Exact calculation of axisymmetric capillary bridge properties between two unequal-sized spherical particles, Math. Mech. Solid (2018). https://doi.org/10.1177/1081286518787842.
- [22] H.N.G. Nguyen, C.F. Zhao>, O. Millet, A.P.S. Selvadurai, Effects of surface roughness on liquid bridge capillarity and droplet wetting, Powder Technol. 378 (2021), https://doi.org/10.1016/j.powtec.2020.10.016.
- [23] D.N. Mazzone, G.I. Tardos, R. Pfeffer, The effect of gravity on the shape and strength of a liquid bridge between two spheres, J. Colloid Interface Sci. 113 (2) (1986), https://doi.org/10.1016/0021-9797(86)90187-6.
- [24] M.J. Matthewson, Adhesion of spheres by thin liquid films, Philos. Mag. A: Physics of Condensed Matter, Structure, Defects and Mechanical Properties 57 (1988) 2, https://doi.org/10.1080/01418618808204510.
- [25] B.J. Ennis, J. Li, T. Gabriel I, P. Robert, The influence of viscosity on the strength of an axially strained pendular liquid bridge, Chem. Eng. Sci. 45 (10) (1990), https:// doi.org/10.1016/0009-2509(90)80054-I.
- [26] O. Pitois, P. Moucheront, X. Chateau, Liquid bridge between two moving spheres: an experimental study of viscosity effects, J. Colloid Interface Sci. 231 (1) (2000), https://doi.org/10.1006/jcis.2000.7096.
- [27] Z. Shi, Y. Zhang, M. Liu, D.A.H. Hanaor, Y. Gan, Dynamic contact angle hysteresis in liquid bridges, Colloids Surf. A Physicochem. Eng. Asp. 555 (2018), https:// doi.org/10.1016/j.colsurfa.2018.07.004.
- [28] M.G. Bozkurt, D. Fratta, W.J. Likos, Capillary forces between equally sized moving glass beads: an experimental study, Can. Geotech. J. 54 (9) (2017), https://doi.org/ 10.1139/cgj-2016-0213.

- [29] K. Pitt, et al., Particle design via spherical agglomeration: a critical review of controlling parameters, rate processes and modelling, Powder Technol. 326 (2018), https://doi.org/10.1016/j.powtec.2017.11.052.
- [30] Y. Kawashima, M. Okumura, H. Takenaka, Spherical crystallization: direct spherical agglomeration of salicylic acid crystals during crystallization, Science 216 (1979) 4550, https://doi.org/10.1126/science.216.4550.1127, 1982.
- [31] A. Lasagabaster, C. Martín, M.M. Goñi, Preparation of spherically agglomerated crystals of the 3,5-diglucoside of cyanidin (cyanin), J. Chem. Technol. Biotechnol. 60 (4) (1994), https://doi.org/10.1002/jctb.280600410.
- [32] A.M. Bailón-Salas, L.A. Ordaz-Díaz, I. Cháirez-Hernández, A. Alvarado-de la Peña, J.B. Proal-Nájera, Lead and copper removal from groundwater by spherical agglomeration using a biosurfactant extracted from Yucca decipiens Trel, Chemosphere 207 (2018), https://doi.org/10.1016/j.chemosphere.2018.05.103.
- [33] A.I. Toldy, et al., Spherical crystallization of glycine from monodisperse microfluidic emulsions, Cryst. Growth Des. 12 (8) (2012), https://doi.org/10.1021/cr200413s
- [34] S. Bindgen, J. Allard, E. Koos, The behavior of capillary suspensions at diverse length scales: from single capillary bridges to bulk, Curr. Opin. Colloid Interface Sci. 58 (2022), https://doi.org/10.1016/j.cocis.2021.101557.
- [35] S.J. Heidlebaugh, T. Domenech, S.v. Iasella, S.S. Velankar, Aggregation and separation in ternary particle/oil/water systems with fully wettable particles, Langmuir 30 (1) (2014), https://doi.org/10.1021/la4039396.
- [36] T. Domenech, S.S. Velankar, On the rheology of pendular gels and morphological developments in paste-like ternary systems based on capillary attraction, Soft Matter 11 (8) (2015), https://doi.org/10.1039/c4sm02053g.
- [37] S. van Kao, L.E. Nielsen, C.T. Hill, Rheology of concentrated suspensions of spheres. II. Suspensions agglomerated by an immiscible second liquid, J. Colloid Interface Sci. 53 (3) (1975), https://doi.org/10.1016/0021-9797(75)90052-1.
- [38] E. Koos, N. Willenbacher, Capillary forces in suspension rheology, Science 331 (1979) 6019, https://doi.org/10.1126/science.1199243, 2011.
- [39] J. Dittmann, E. Koos, N. Willenbacher, Ceramic capillary suspensions: novel processing route for macroporous ceramic materials, J. Am. Ceram. Soc. 96 (2) (2013). https://doi.org/10.1111/jace.12126.
- [40] J. Maurath, N. Willenbacher, 3D printing of open-porous cellular ceramics with high specific strength, J. Eur. Ceram. Soc. 37 (15) (2017), https://doi.org/10.1016/ i.jeurceramsoc.2017.06.001.
- [41] H. Sun, X. Zhang, M.M.F. Yuen, Enhanced conductivity induced by attractive capillary force in ternary conductive adhesive, Compos. Sci. Technol. 137 (2016), https://doi.org/10.1016/j.compscitech.2016.10.028.
- [42] D. Amoabeng, S.S. Velankar, Bulk soldering: conductive polymer composites filled with copper particles and solder, Colloids Surf. A Physicochem. Eng. Asp. 553 (2018), https://doi.org/10.1016/j.colsurfa.2018.06.013.
- [43] W.B. Russel, Formulation and processing of colloidal dispersions, MRS Proceedings 177 (1989), https://doi.org/10.1557/proc-177-281.
- [44] Y.I. Rabinovich, M.S. Esayanur, B.M. Moudgil, Capillary forces between two spheres with a fixed volume liquid bridge: theory and experiment, Langmuir 21 (2005) 24, https://doi.org/10.1021/la0517639.
- [45] D. Megias-Alguacil, L.J. Gauckler, Analysis of the capillary forces between two small solid spheres binded by a convex liquid bridge, Powder Technol. 198 (2) (2010), https://doi.org/10.1016/j.powtec.2009.11.009.
- [46] M. Wagner, B.A. Wolf, Interfacial tension between poly(isobutylene) and poly(dimethylsiloxane): influence of chain length, temperature, and solvents, Macromolecules 26 (1993) 24, https://doi.org/10.1021/ma00076a029.
- [47] X. Zhang, R.S. Padgett, O.A. Basaran, Nonlinear deformation and breakup of stretching liquid bridges, J. Fluid Mech. 329 (1996), https://doi.org/10.1017/ S0022112096008907
- [48] F. Soulié, M.S. el Youssoufi, F. Cherblanc, C. Saix, Capillary cohesion and mechanical strength of polydisperse granular materials, European Physical Journal E 21 (4) (2006), https://doi.org/10.1140/epje/i2006-10076-2.
- [49] G. Lian, C. Thornton, M.J. Adams, A theoretical study of the liquid bridge forces between two rigid spherical bodies, J. Colloid Interface Sci. 161 (1) (1993), https://doi.org/10.1006/jcis.1993.1452.
- [50] S.S. Velankar, A non-equilibrium state diagram for liquid/fluid/particle mixtures, Soft Matter 11 (2015) 43, https://doi.org/10.1039/c5sm01901j.